Locally Rigid Globally Non-rigid Surface Registration

Kent Fujiwara[1], Ko Nishino[2], Jun Takamatsu[3], Bo Zheng[1] and Katsushi Ikeuchi[1]
[1]Institute of Industrial Science, The University of Tokyo
[2]Department of Computer Science, Drexel University
[3]Graduate School of Information Science, Nara Institute of Science and Technology
[1]{kfuji,zheng,ki}@cvl.iis.u-tokyo.ac.jp [2]kon@drexel.edu [3]j-taka@naist.jp

Abstract

We present a novel non-rigid surface registration method that achieves high accuracy and matches characteristic features without manual intervention. The key insight is to consider the entire shape as a collection of local structures that individually undergo rigid transformations to collectively deform the global structure. We realize this locally rigid but globally non-rigid surface registration with a newly derived dual-grid Free-form Deformation (FFD) framework. We first represent the source and target shapes with their signed distance fields (SDF). We then superimpose a sampling grid onto a conventional FFD grid that is dual to the control points. Each control point is then iteratively translated by a rigid transformation that minimizes the difference between two SDFs within the corresponding sampling region. The translated control points then interpolate the embedding space within the FFD grid and determine the overall deformation. The experimental results clearly demonstrate that our method is capable of overcoming the difficulty of preserving and matching local features.

1. Introduction

The goal of non-rigid surface registration is to deform the surface of a source shape to match the surface of a target shape. Non-rigid registration finds many applications in a wide range of areas including object modeling [2], and medical imaging [11, 19]. Non-rigid registration is, however, very challenging as an infinite number of solutions may exist. Past research on non-rigid registration has mainly focused on imposing appropriate regularization on the deformation to arrive at unique solutions [3].

We claim that an *ideal* surface registration should match characteristic features on the source shape to the corresponding features on the target shape. Prior work has attempted to accomplish this mainly by explicitly identifying corresponding features either by manual intervention or by feature extraction [4].

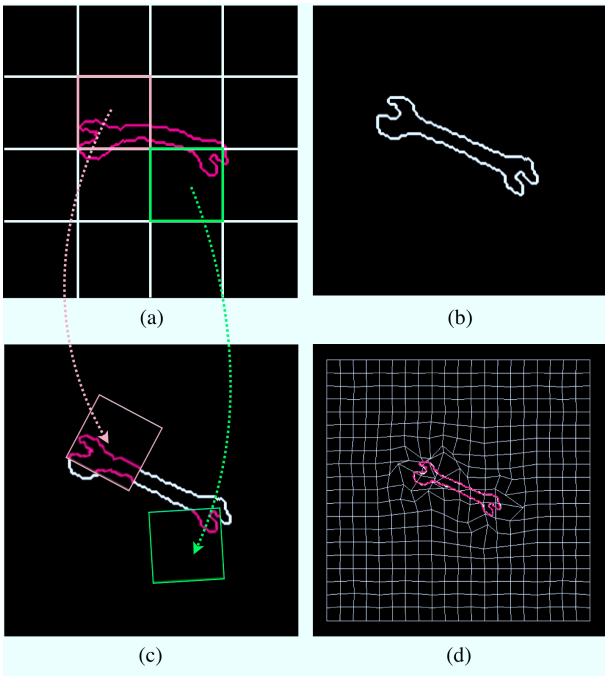

Figure 1. Our method deforms a source shape (a) to the target shape (b) by rigidly aligning local structures (c) that collectively form a free form deformation grid in a coarse-to-fine fashion (d).

We search for this *ideal* registration by computing a shape-preserving deformation that brings the original shape into alignment with the target shape. We build on the key insight that the entire shape can be considered as a collection of local structures, each of which transforms rigidly to align with counterparts of the target shape and collectively deform the overall global structure. That is, we try to retain the local structures that determine the characteristics of the shape by guiding the deformation with the rigid movements of local structures to match the target as a whole.

We adopt an implicit shape representation, the signed distance field (SDF), to represent the shapes and the space

around the surfaces (Section 3). We also define a similarity metric between two SDFs that describes the spatial difference between the source and the target shapes (Section 4).

To go along with this spatial similarity metric, we choose to represent the deformation using a spatial deformation method, namely, free-form deformation (FFD) [14]. By surrounding the source shape with a control point grid, we are able to model and visualize the spatial deformation required to match the surface of the source shape to the surface of the target shape.

We propose a novel dual-grid FFD representation to achieve the locally rigid, globally non-rigid registration. The secondary grid, which we call the sampling grid, is superimposed over the FFD control point grid that controls the overall deformation. The sampling grid is subdivided into sampling regions so that each control point is enclosed by one sampling region. Each sampling region acts as a guide for finding the optimal translation of the control point within. The control point is translated based on the rigid transformation required to minimize the difference between the signed distance fields in the corresponding sampling region. Deformation is determined by the new positions of the control points (Section 4).

We demonstrate the effectiveness of the method through a number of experiments using 2D contour images (Section 5). We also show that the method can easily be extended to handle 3D range data (Section 6). The results show that our method can match the overall shape and at the same time establish accurate correspondences of local features. This characteristic is desirable for many applications of non-rigid registration as it enables meaningful shape comparison and analysis.

2. Related Work

Non-rigid registration has long been an active area of research due to its applicability to various fields. Most of the work on non-rigid registration mainly focuses on defining the similarity between shapes and introducing regularization on deformation. We refer the readers to surveys [7, 11, 20] for thorough introduction to general non-rigid registration methods.

Shape-preserving non-rigid registration is starting to be considered as an important method to obtain accurate correspondences between two shapes. There have been various attempts to obtain deformation capable of maintaining the features. Thirion [16] and Vercauteren *et al*. [18] proposed methods to obtain smooth deformation field in order to avoid any folding or tearing. Recently, Oxholm and Nishino [9] proposed a Gaussian mixture-based method with novel energy terms introduced to preserve local shapes. However, their method targets 2D intensity images, and it is unclear how it can be applied to 2D contour or 3D surface data.

Free-form deformation (FFD) [14] is a deformation method where an object is embedded inside a grid consisting of control points. The space and the object inside the grid is deformed by moving the control points of the FFD grid. This deformation method has been used extensively for image and shape registration. Rueckert *et al*. [13] maximizes the mutual information, which is used as the similarity metric for deformation. Rohlfing *et al*. [12] introduced an incompressibility constraint to preserve the volume of the image for smooth deformation. Although FFD is used to model local deformations, local rigidity is also significant for retaining local features of the object being deformed. We propose to achieve this by introducing a locally rigid sampling grid over the conventional FFD grid. The rigid transformation of each sampling region on the sampling grid is obtained through minimization of the difference between two SDFs.

Recently, implicit shape representation has gained attention in various fields [5], including registration. Paragios *et al*. [10] proposed a global-to-local registration framework using distance functions. Huang *et al*. [4] extended this method by introducing an initial registration step and a local non-rigid registration by FFD based on signed distance fields. Munim and Farag [8] proposed to use the vector distance function instead of the signed distance function. These methods are similar to our method since they attempt to spatially register two shapes through optimization of spatial information. These methods, however, do not automatically find deformations that match characteristic local features. Huang *et al*. manually selected feature points on both the source and the target images to identify a deformation that aligns those correspondences. Local rigidity serves to preserve and match such local structures without any manual intervention.

3. Shape Representation

We first compute an implicit representation of the source and target shapes using the signed distance field (SDF). For the sake of simplicity, we explain this for 2D shapes but the same computation easily extends to 3D shapes.

Given a data shape $\mathbf{A}$, we consider an arbitrary point $\mathbf{x}$. From this arbitrary point, we search for the closest point on the data shape $\mathbf{A}$, which we denote as $\mathbf{a_x} \in \mathbf{A}$. We assume that the surface normal of the shape is available at this point, which is expressed as $\mathbf{n_{a_x}}$. The signed distance $\phi_{\mathbf{A}}(\mathbf{x})$ of point $\mathbf{x}$ to the shape $\mathbf{A}$ is defined as the normal projected distance

$$\phi_{\mathbf{A}}(\mathbf{x}) = \mathbf{n}_{\mathbf{a_x}}^T(\mathbf{x} - \mathbf{a_x})\,. \tag{1}$$

One drawback of using the implicit representation is the increase in data. In other works that use the implicit representation, the field far from the object surface is omit-

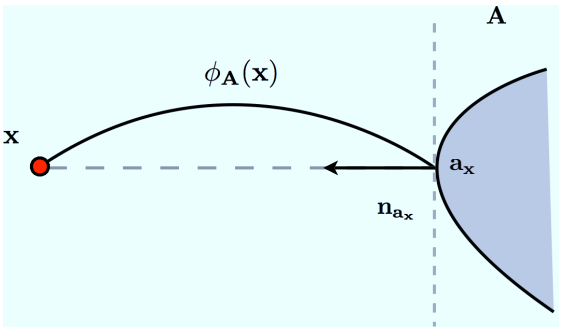

Figure 2. The signed distance is calculated by finding the closest point from the point $\mathbf{x}$ and the normal of the closest point.

ted from the registration process to reduce computational cost (i.e., narrow-band representation). We, however, do not omit any of the parts of the field in order to maintain the consistency between local rigidity and global deformability. We, instead, sample the space for faster calculation of distance fields. We spread the sampling points in the space evenly. By calculating the signed distance at uniformly spread sampling points, we produce the SDF $\mathbf{\Phi_A}$ around the shape $\mathbf{A}$.

4. Local Rigidity, Global Deformability

We propose a dual-grid FFD framework to achieve locally rigid and globally non-rigid deformation. Figure 3 illustrates the overview of this framework. Here, we consider a registration process between a source shape $\mathbf{A}$ consisting of points $\mathbf{a} \in \mathbf{A}$ and a target shape $\mathbf{B}$ consisting of points $\mathbf{b} \in \mathbf{B}$. First, as in other methods using FFD, we prepare a grid that surrounds the source shape $\mathbf{A}$, which will be deformed in this process. This grid consists of FFD control points whose locations control the deformation of the field within. In Figure 3, the FFD grid is shown as a gray grid.

In addition to this FFD grid, we add another grid, which we refer to as the sampling grid. We define each block of this sampling grid as sampling region $\mathbf{S}$ consisting of sampling points $\mathbf{s}$. In Figure 3, this grid is shown in red. The sampling grid is defined relative to the FFD grid so that a single FFD control point $\mathbf{P}_i$ is immersed in a single sampling region $\mathbf{S}_{\mathbf{P}_i}$. This is achieved by defining the sampling region for each FFD control point by connecting the midpoints of the edges of the FFD grid connected to the control point of interest. This ensures that the sampling regions will be mutually exclusive and no space is sampled more than once. We place the same number of sampling points $\mathbf{s}$ and space them uniformly within each sampling region by defining them relative to the midpoints of the control points at the corners of the sampling region. This is to ensure that each region is thoroughly sampled even when the deformation of the FFD grid alters the shape of sampling regions.

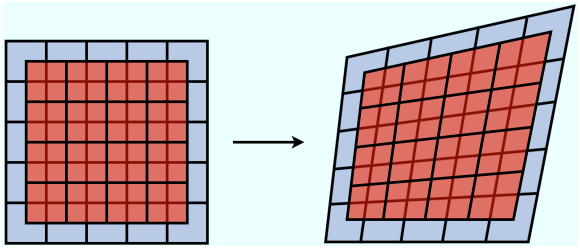

Figure 3. The sampling grid (red) is placed over the conventional FFD control point grid (gray). Each sampling region $\mathbf{S}$ transforms rigidly, moving the underlying control point $\mathbf{P}$ embedded within. The sampling grid is defined relative to the FFD grid so that the sampling grid completely covers the FFD grid without any overlap even after the FFD grid is deformed.

4.1. Local Rigid Registration

In this method, we consider each sampling region as a rigid space that moves independently in order to minimize the difference of the SDFs within each region. These local rigid transformations will then be consolidated to form a global deformation through the FFD control points. The error function for a sampling region $\mathbf{S}$ can then be written as the sum of the distances across all the points $\mathbf{s} \in \mathbf{S}$

$$E = d(\mathbf{\Phi_A}, \mathbf{\Phi_B}) = \sum_{\mathbf{s} \in \mathbf{S}} \Big(\phi_{\mathbf{B}}(\mathbf{s}) - \phi_{\mathbf{A}}(\mathbf{s}) \Big)^2 . \quad (2)$$

We solve for the optimal rigid transformation for each sampling region $\mathbf{S_P}$ that minimizes the above error function. To register the two SDFs, we use the iterative registration method proposed by Lucas and Kanade [6]. We solve for the optimal transformation that minimizes the difference between the SDF of the source image and the SDF of the target image, which is warped onto the coordinate frame of the source image. The energy function would then be written as

$$E = \sum_{\mathbf{s}} \Big(\phi_{\mathbf{B}}\Big(\mathbf{T}(\mathbf{s}; \mathbf{w})\Big) - \phi_{\mathbf{A}}(\mathbf{s}) \Big)^2 , \quad (3)$$

where $\mathbf{T}$ is the transformation function and $\mathbf{w}$ represents the transformation parameters. In the case of 2 dimensional images, the parameters consist of translations $\mathbf{t_s} = (t_x, t_y)$ and the angle of rotation θ about the origin (i.e., the corresponding control point of the sampling region). The Lucas-Kanade algorithm iteratively solves for the increments in the parameters $\Delta\mathbf{w}$ and updates the estimated parameters $\mathbf{w}$ by solving for the error function redefined as

$$E = \sum_{\mathbf{s}} \Big(\phi_{\mathbf{B}}\Big(\mathbf{T}(\mathbf{s}; \mathbf{w} + \Delta\mathbf{w})\Big) - \phi_{\mathbf{A}}(\mathbf{s}) \Big)^2 . \quad (4)$$

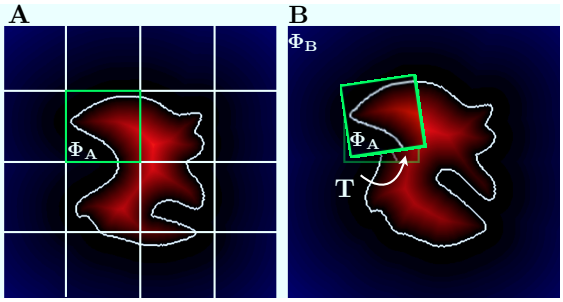

Figure 4. The difference between the signed distance field $\mathbf{\Phi_A}$ of the sampling region of the source image $\mathbf{A}$ and the signed distance field $\mathbf{\Phi_B}$ of the target image $\mathbf{B}$ is minimized by the rigid transformation $\mathbf{T}$ of the sampling region. This transformation guides the movement of the FFD control point, which determines the overall global deformation in the following step.

Taylor expansion can be used to linearize this expression

$$E = \sum_{\mathbf{s}} \left(\phi_{\mathbf{B}}\Big(\mathbf{T}(\mathbf{s};\mathbf{w})\Big) + \nabla\phi_{\mathbf{B}} \frac{\partial \mathbf{T}}{\partial \mathbf{w}} \Delta\mathbf{w} - \phi_{\mathbf{A}}(\mathbf{s}) \right)^2 , \quad (5)$$

where $\nabla\phi_{\mathbf{B}}$ represents the gradient of the signed distance. We use the unit vector directed from the transformed sampling point to the object surface. The partial derivative of the error function with respect to $\Delta\mathbf{w}$ is

$$\frac{\partial E}{\partial \Delta\mathbf{w}} = 2 \sum_{\mathbf{s}} \left[\nabla\phi_{\mathbf{B}} \frac{\partial \mathbf{T}}{\partial \mathbf{w}} \right]^{\mathbf{T}} \left[\phi_{\mathbf{B}}\Big(\mathbf{T}(\mathbf{s};\mathbf{w})\Big) + \nabla\phi_{\mathbf{B}} \frac{\partial \mathbf{T}}{\partial \mathbf{w}} \Delta\mathbf{w} - \phi_{\mathbf{A}}(\mathbf{s}) \right] . \quad (6)$$

This yields the additional values to the parameters $\Delta\mathbf{w}$

$$\Delta\mathbf{w} = \mathbf{H}^{-1} \sum_{\mathbf{s}} \left[\nabla\phi_{\mathbf{B}} \frac{\partial \mathbf{T}}{\partial \mathbf{w}} \right]^{\mathbf{T}} \left[\phi_{\mathbf{A}}(\mathbf{s}) - \phi_{\mathbf{B}}\Big(\mathbf{T}(\mathbf{s};\mathbf{w})\Big) \right] , \quad (7)$$

where $\mathbf{H}$ is the Gauss-Newton approximation to the Hessian matrix which can also be written as

$$\mathbf{H} = \sum_{\mathbf{s}} \left[\nabla\phi_{\mathbf{B}} \frac{\partial \mathbf{T}}{\partial \mathbf{w}} \right]^{\mathbf{T}} \left[\nabla\phi_{\mathbf{B}} \frac{\partial \mathbf{T}}{\partial \mathbf{w}} \right] . \quad (8)$$

There are cases where the Hessian matrix is ill-conditioned. This is likely to happen when the sampling region is away from the object surface and the signed distance field inside the region does not contain much information concerning the surface. The sampling region with the ill-conditioned Hessian can disturb the overall registration result. We allow the movement of control points whose Hessian's condition number is within the bottom 15 percent of all the control points and do not update the rest of the control points.

In the final step, we update the parameters by adding the incremental values to the initial parameters $\mathbf{w} + \Delta\mathbf{w}$. This rigid registration process is conducted until convergence is obtained for each of the sampling regions.

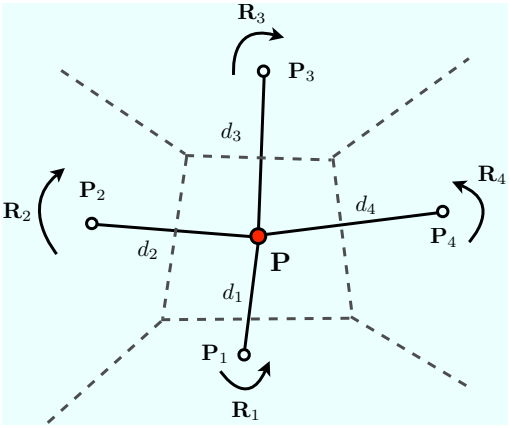

Figure 5. The control point at the center $\mathbf{P}$ is also translated by the rotations computed for neighboring control points from their corresponding sampling regions.

In this process, we solved for the rigid transformation of each sampling region that minimizes the difference of corresponding SDFs. It is worth noting that we do not at any point consider that the space within each sampling region stays rigid. The rigid transformation obtained in this process only guides the movement of the FFD control points, which determines the overall deformation.

Deformation is defined by the coordinates of the control points on the FFD grid. The translation vector can therefore be applied to move the control points, but the rotation, which rotates the sampling region around the control point, has no effect on the displacement of its center, that is, the control point itself. We realize the rotation computed from a sampling region of a single FFD control point by rotating the local coordinate frame with its origin at the control point. This means that the rotation computed for a single control point must rotate the four neighboring control points around that point, and in turn the control point must be rotated around each of the neighboring control points by the rotation computed from corresponding sampling regions. Figure 5 illustrates the neighborhood which influences each control point. To include the effect that a control point receives from the neighboring n control points, we convert the rotation of neighboring control points $\mathbf{R}_i$ into translation $\mathbf{t_R}$ of the control point at the center $\mathbf{P}$

$$\mathbf{t_R} = \sum_{i}^{n} w_d \mathbf{R}_i (\mathbf{P} - \mathbf{P}_i) , \quad (9)$$

where $w_d = \frac{w_i}{\sum_j^n w_j}$ is the weight based on the distance between the control points and $w_i = \frac{\sum_k^n d_k}{d_i}$ is the inverse of the normalized distance. d_i represents the distance between

the control point at the center $\mathbf{P}$ and the neighboring control point $\mathbf{P}_i$. The weight term is introduced based on the basic notion that the closer a sampling region is, the more the control point $\mathbf{P}$ should be influenced by it. This assigns more weight to the control points $\mathbf{P}_i$ that are closer to $\mathbf{P}$. The weights are normalized so that the total of the neighbor weights sum to one to avoid excessive effect from control points that are very close to each other.

4.2. Global Non-rigid Registration

We apply the rigid transformation obtained from each sampling region to the corresponding control point. Using these coordinates we move the FFD grid and apply the FFD deformation to the source shape. This process of computing the rigid transformation locally and applying it to the control points to deform globally is iterated until convergence.

Deformation of a point $\mathbf{a} = (x, y)$ using cubic B-spline FFD is computed by the weighted sum of the translations of the control points

$$\mathbf{F}(\mathbf{a}) = \sum_i \sum_j B_i(u) B_j(v) \mathbf{P}\,, \tag{10}$$

where B denotes the B-spline basis function and u, v represent the relative coordinates of x and y within the FFD grid.

The global deformation of the point $\mathbf{a}$ on the surface $\mathbf{A}$ is obtained by adding the translations $\mathbf{t_s}$ and $\mathbf{t_R}$ to the coordinates of the control points

$$\begin{aligned} \mathbf{F}(\mathbf{a}) \quad = \quad & \sum_i \sum_j B_i(u) B_j(v) \\ & \Big(\mathbf{P} + \alpha_{\mathbf{S_P}} (\mathbf{t}_{\mathbf{s},i,j} + \mathbf{t}_{\mathbf{R},i,j}) \Big)\,. \end{aligned} \tag{11}$$

When computing the translation of a control point from its sampling region, we weight the influence of the sampling region according to the area using the weight α. This ensures that if the sampling region, which is defined relatively to the FFD grid, becomes smaller in the course of iterative computation of the deformation, its influence is lessened and eventually vanishes if it becomes degenerate. Therefore, α becomes smaller when the area of the sampling region $\mathbf{S}$ is smaller, and becomes larger when $\mathbf{S}$ is larger

$$\alpha_{\mathbf{S_P},k} = \frac{S_{\mathbf{P},k}}{S_{\mathbf{P},0}}\,, \tag{12}$$

where $S_{\mathbf{P},0}$ and $S_{\mathbf{P},k}$ are the area of sampling region around $\mathbf{P}$ at the initial stage and at the k-th iteration. This is normalized by dividing it by the largest value α_m

$$\alpha_{\mathbf{S_P},k} = \frac{\alpha_{\mathbf{S_P},k}}{\alpha_m}\,. \tag{13}$$

5. Experimental Results

We evaluate the proposed method on 2D images using the silhouette data from the database provided by Sharvit *et al*. [15] and Bronstein *et al*. [1]. We extracted the contour data from these silhouette images and used them to test the registration accuracy. We compared the result of our method with the results of the distance-based method by Huang *et al*. [4]. First, we obtained the results from Huang *et al*.'s method without the feature constraint. We then gave explicit feature correspondences to Huang *et al*.'s method and adjusted the parameters, such as the weight on the feature constraint and the bandwidth of SDFs, to acquire the best possible registration results. The feature points that were provided are marked as blue dots on the source and the target image. These features are not given to our method, and are just used to quantitatively evaluate the registration accuracy. We also marked other features that were not given to any of the methods. These points, which are marked as pink dots, are also used to evaluate the accuracy of registration to gauge whether each method is capable of matching characteristic structures without explicit assignment of feature correspondences. For Huang *et al*.'s method with the feature constraint, this evaluates whether the registration computed from the given feature correspondences can propagate to align other features that were not specified. The corresponding features on the target surface are marked as white dots for visualization. In this section we present the registration results of "Device," "Fgen," "Misk," "Fish," and "Dude" from the database of Sharvit *et al*. [15] and "Pliers" and "Scissors" from the database of Bronstein *et al*. [1].

We used the same number of control points for the FFD grid in all of the methods. Huang *et al*.'s method uses a coarse-to-fine approach and subdivides the FFD grid once the registration converges in the coarse stage. We applied the same approach to all the methods for comparison.

The registration results are shown in Figure 6. Figure 7 shows the residual error between all the feature points. In the case of Figure 6 (a), the previous methods come close to successful registration. However, the marked feature points did not match precisely. The result from our method is very accurate. Although these two shapes are quite different from each other, the assumption of local rigidity maintained the relative positions of the features and successfully matched them to the corresponding features.

In case of Figure 6 (b), our method, the method by Huang *et al*. with the feature constraint and the featureless version of Huang *et al*.'s method performed well and matched the surfaces and the blue feature points. At the same time, our method was able to accurately register the pink non-feature points. These two examples show that our method treats all the locations on the surface evenly and automatically achieves feature correspondence without any a priori correspondences.

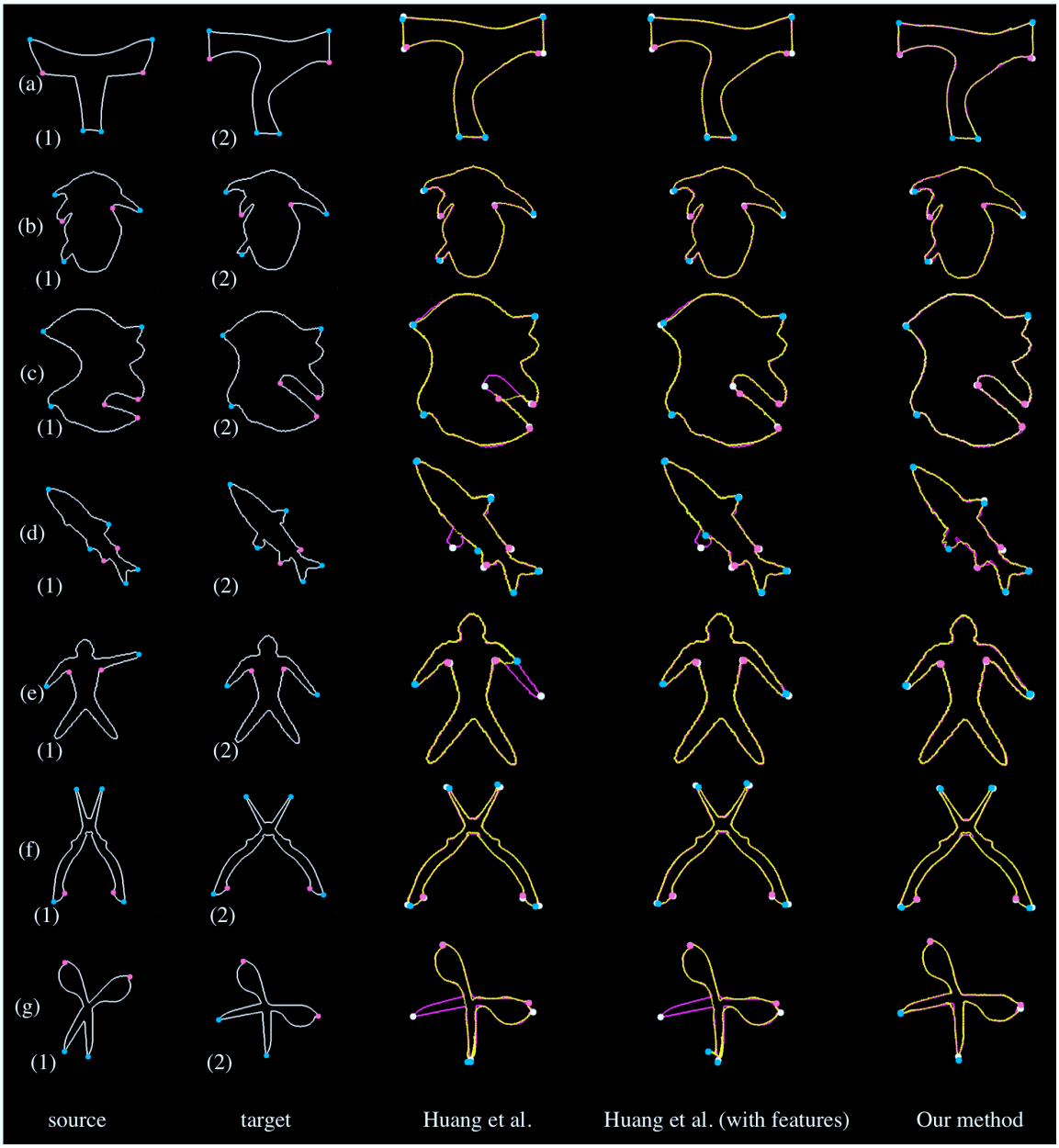

Figure 6. Contour data from the database by Sharvit *et al*. [15] and Bronstein *et al*. [1] were used to evaluate the accuracy of the proposed method: (a) Device, (b) Fgen, (c) Misk, (d) Fish, (e) Dude, (f) Pliers, and (g) Scissors. The source images (1) were registered to the target images (2). The accuracy of the method by Huang *et al*., even with the explicit features, lowered as the local structure of the shapes became complex. Our method was successful in all the cases.

In the case of Figure 6 (c), even though the previous methods succeeded in matching the outer surface and the blue features, the featureless version was stuck at a local minimum. Huang *et al*.'s method using the features managed to match the inner surface, but the pink feature point inside the opening failed to match. Our method precisely matched this structure. In the case of Figure 6 (d), both the Huang *et al*.'s method with or without the feature constraint failed to match one of the fins that was designated as a feature. Our method successfully matches the shapes even without any information of feature correspondence.

In Figure 6 (e), our method and the method by Huang *et al*. with the feature constraint performed well and matched the surfaces. The featureless version of the method by

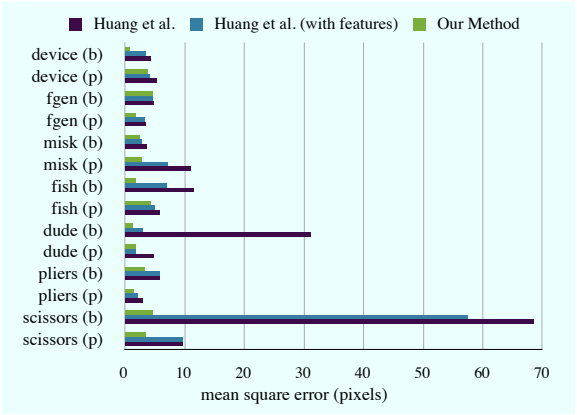

Figure 7. The mean square error between the blue feature points (b) and pink feature points (p) indicates that our method constantly outperforms other methods.

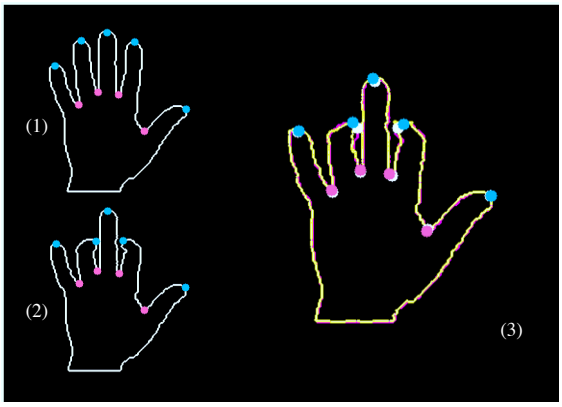

Figure 8. The source image (1) of "Hand" was deformed to the target image (2). Although the registration (3) is successful in terms of contour matching, the fingertips on the deformed hand did not quite match the fingertips of the normal hand due to the limitation of acquiring features from contours.

Huang *et al*. was stuck at a local minimum. The right arm of the image was difficult to register for the method by Huang *et al*. even with the given features, and required additional weight on the feature correspondences. However, this manual operation was still not enough to match the features on the right arm. This example shows that depending on the shape being registered, the method by Huang *et al*. requires manual parameter setting, as well as manual feature selection. Our method automatically achieves feature correspondence without any a priori correspondences by preserving the local features through local rigidity.

In Figure 6 (f), the previous methods were able to register the surfaces to some extent, but the accuracy was still better in our method. The previous methods failed in the case of Figure 6 (g), where one of the blades could not be registered to the corresponding part. We tried adding extra weight to the Huang *et al*.'s feature constraint, but could not find the proper parameter that would allow the corresponding parts to match. Our method was able to match the features together with the assumption of local rigidity and register the entire surface.

Figure 8 shows the registration result of the shape "Hand" using the proposed method. Our method was successful at registering the two contours. However, the blue points, which are manually placed on what seemed to be the fingertips for evaluation of accuracy, did not completely move to the corresponding fingertips. This is due to the limitation of providing ground truth since it is hard for even a person to identify where the fingertips are in the images.

These results have demonstrated that our method is able to deform the source shape to align with the target shape, while preserving and matching characteristic features of the shapes. This has been conducted automatically, without any feature correspondences or manual intervention.

6. Extension to 3D

Extending our method to handle 3D surface data is straightforward. We add the third coordinate z to the vectors and matrices shown in Section 4. The area of the sampling region used for calculating the weight α for global deformation is replaced with the volume of the 3D sampling volume. The rest of the method is the same as in 2D.

We have tested the 3D version of our method with synthetic 3D range data of a wave and a deformed version of the wave. Figure 9 (a) shows the registration results. Although initial globally rigid registration leaves behind a large gap between the two shapes at two of the corners, our method was able to register them accurately through the locally rigid but globally non-rigid registration. In Figure 9 (b), we randomly deformed the "Stanford Bunny" [17] and registered the original model to the deformed model. Although large deformations were applied to the ears and the back, our method was able to match the corresponding parts. We also processed 3D data taken from two separate chicken skulls to test our method on real data. Figure 9 (c) is the result of registration. Although there is a gap between the beaks at the initial stage, the locally rigid globally non-rigid registration successfully aligns them. The experiments on synthetic and real data in 3D demonstrate that the method is effective in 3D as well.

7. Conclusion

Our concept of "align locally, deform globally" is based on the key idea that the shape along with the distance fields around it should maintain rigidity even in a non-rigid registration framework. Our method based on this key idea proved to be very effective in preserving local features

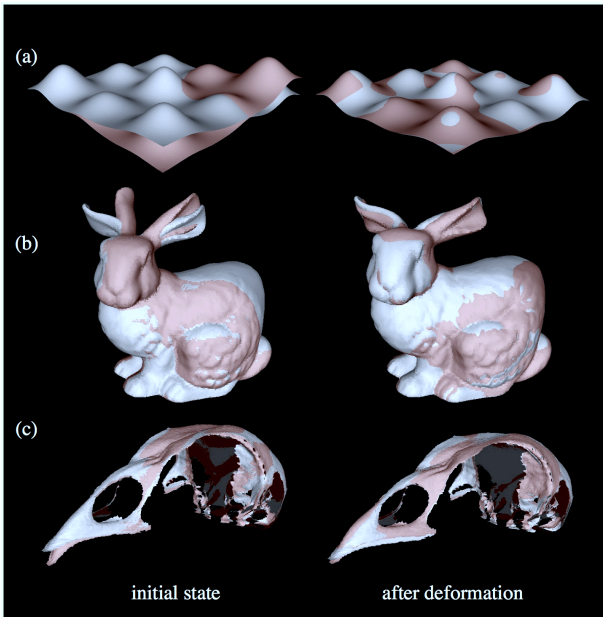

Figure 9. The method was applied to 3D synthetic data of waves (a), "Stanford Bunny" (b), and real data taken from actual skulls of chicken (c). The source image (red) was deformed to match the target image (white). Our method was successful at matching parts that were apart after initial rigid registration.

and matching them to corresponding features on the target, which we believe is the most important aspect in non-rigid registration.

The experimental results have demonstrated the effectiveness of our method in most cases, and both the overall accuracy and feature correspondence has been achieved. Even in cases where initial alignment is difficult to conduct, the registration was accomplished successfully. All of this has been achieved without manual intervention.

Acknowledgements

This work was supported in part by National Science Foundation awards CAREER IIS-0746717 and IIS-0803670, and the Office of Naval Research grant N00014-11-1-0099 to KN, and Ministry of Education, Culture, Sports, Science and Technology under Digital Museum Project to KI.

References

[1] A. Bronstein, M. Bronstein, A. Bruckstein, and R. Kimmel. Analysis of two-dimensional non-rigid shapes. *International Journal of Computer Vision*, 78(1):67 – 88, 2008.

[2] B. J. Brown and S. Rusinkiewicz. Global non-rigid alignment of 3-d scans. *ACM Trans. on Graphics*, 26, 2007.

[3] H. Chui and A. Rangarajan. A new point matching algorithm for non-rigid registration. *Computer Vision and Image Understanding*, 89(2-3):114 – 141, 2003.

[4] X. Huang, N. Paragios, and D. Metaxas. Shape registration in implicit spaces using information theory and free form deformations. *IEEE Trans. on Pattern Analysis and Machine Intelligence*, 28(8):1303–1318, 2006.

[5] M. Jones, J. Bærentzen, and M. Sramek. 3d distance fields: A survey of techniques and applications. *IEEE Trans. on Visualization and Computer Graphics*, 12(4):581–599, 2006.

[6] B. Lucas and T. Kanade. An iterative image registration technique with an application to stereo vision. In *Proc. of International Joint Conference on Artificial Intelligence*, pages 674–679, 1981.

[7] J. Maintz and M. Viergever. A survey of medical image registration. *Medical Image Analysis*, 2(1):1 – 36, 1998.

[8] H. E. Munim and A. Farag. Shape representation and registration using vector distance functions. In *Proc. of IEEE Conf. on Computer Vision and Pattern Recognition*, pages 1 –8, 2007.

[9] G. Oxholm and K. Nishino. Membrane nonrigid image registration. In *Proc. of 11th European Conference on Computer Vision*, volume 6312, pages 763–776, 2010.

[10] N. Paragios, M. Rousson, and V. Ramesh. Non-rigid registration using distance functions. *Computer Vision and Image Understanding*, 89(2-3):142 – 165, 2003.

[11] J. Pluim, J. Maintz, and M. Viergever. Mutual-information-based registration of medical images: a survey. *IEEE Trans. on Medical Imaging*, 22(8):986 – 1004, 2003.

[12] T. Rohlfing, C. M. Jr., D. Bluemke, and M. Jacobs. Volume-preserving nonrigid registration of mr breast images using free-form deformation with an incompressibility constraint. *IEEE Trans. on Medical Imaging*, 22(6):730 –741, 2003.

[13] D. Rueckert, L. Sonoda, C. Hayes, D. Hill, M. O. Leach, and D. Hawkes. Nonrigid registration using free-form deformations: Application to breast mr images. *IEEE Trans. on Medical Imaging*, 18(8):712 – 721, 1999.

[14] T. Sederberg and S. Parry. Free-form deformation of solid geometric models. *Proc. of ACM SIGGRAPH*, 20(4):151 – 160, 1986.

[15] D. Sharvit, J. Chan, H. Tek, and B. Kimia. Symmetry-based indexing of image databases. *Journal of Visual Communication and Image Representation*, 9(4):366–380, 1998.

[16] J.-P. Thirion. Non-rigid matching using demons. In *IEEE Conf. on Computer Vision and Pattern Recognition*, pages 245 – 251, 1996.

[17] G. Turk and M. Levoy. Zippered polygon meshes from range images. *Proc. of ACM SIGGRAPH '94*, pages 311 – 318, 1994.

[18] T. Vercauteren, X. Pennec, A. Perchant, and N. Ayache. Diffeomorphic demons: Efficient non-parametric image registration. *NeuroImage*, 45(1, Supplement 1):S61 – S72, 2009.

[19] W. Zeng, D. Samaras, and X. D. Gu. Ricci flow for 3d shape analysis. *IEEE Trans. on Pattern Analysis and Machine Intelligence*, 32(4):662–677, 2010.

[20] B. Zitová and J. Flusser. Image registration methods: a survey. *Image and Vision Computing*, 21(11):977 – 1000, 2003.